Available online at www.synsint.com

Synthesis and Sintering

ISSN 2564-0186 (Print), **ISSN** 2564-0194 (Online)

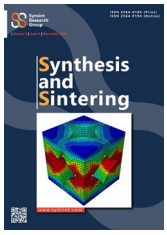

Research article

Investigation of the sintering behavior of SiC-5TiB_2 composites reinforced by graphene quantum dots

Maryam Nazari, Hamid Reza Baharvandi *, Nasser Ehsani

Faculty of Materials & Manufacturing Technologies, Malek Ashtar University of Technology, Tehran, Iran

ABSTRACT

The purpose of this research is to fabricate and investigate the properties of SiC-5TiB_2 nano composites reinforced with graphene quantum dot nanoparticles by a pressureless sintering method. In this way, SiC, TiB_2, and graphene quantum dots were used in nanometer dimensions. First, before performing any laboratory operation, the thermodynamic behavior of the system was checked using HSC software. The graphene quantum dots reinforcement amount was 0.6 wt%, and the sinter temperature was defined as 2000, 2050, 2100, 2150, and 2200 °C. After weighing the initial powders, the grinding process was carried out in an ethanol-based wet environmental and a polymer chamber, using zirconia balls, for two hours at a speed of 200 rpm. The sintering process was also carried out at certain temperatures in an argon atmosphere for two hours. Then, XRD, FESEM, and Raman analyses were performed, and density, microhardness, and fracture toughness tests were used for further investigations. The microstructure of the samples was also investigated to investigate the fracture toughness mechanisms. The results show that the sample sintered at 2150 °C with a relative density of 96.26%, and a hardness of 28.65 GPa and a fracture toughness of 4.1 MPa.$m^{1/2}$ is the best case.

KEYWORDS

SiC
Graphene quantum dot
Composite
Pressureless sintering
Mechanical properties

OPEN ACCESS

1. Introduction

Ultra-high temperature ceramics (UHTCs) are a group of materials known for their exceptional mechanical and physical properties, including a high melting point, good wear resistance, high elastic modulus, notable hardness, excellent thermal and electrical conductivity, outstanding chemical stability, and good oxidation resistance. These materials are utilized in various fields, such as thermal protection structures for space vehicles, refractory crucibles, plasma arc electrodes, and rocket engines. UHTCs can be divided into three main groups: oxides, carbides, and borides [1–6].

Among these, silicon carbide (SiC) exhibits excellent mechanical and physical properties, remarkable wear resistance, and good thermal stability at elevated temperatures (up to 1500 °C) [4–8]. Due to these attributes, silicon carbide is widely used in thermal equipment, refractory applications, thermocouple protectors, substitutes for superalloys, and advanced military industries [4, 9–11]. However, the poor fracture toughness and variability in the mechanical properties of SiC limit its wider application [3–5].

Titanium diboride (TiB_2), another member of UHTCs, possesses interesting characteristics and is extensively used in cutting tools, seals, aerospace applications, armor, and crucibles due to its high melting point, high hardness, and good thermal and electrical conductivity [11–15]. Nevertheless, due to intrinsic properties such as poor self-diffusion coefficients, strong covalent bonds, and a very high melting point, manufacturing porosity-free TiB_2 compounds through conventional methods like powder metallurgy remains challenging. Furthermore, the inherent brittleness of purely sintered titanium diboride, combined with low sinterability, poses obstacles to its application in certain areas [16–23]. In contrast, the primary TiB_2 powder particles are naturally covered by oxide compounds, which negatively impact the aggregation process [24–27]. These oxide compounds, primarily TiB_2 and B_2O_3,

* Corresponding author. *E-mail address:* H.R.Baharvand@gmail.com (H.R. Baharvandi)
Received 21 October 2025; Received in revised form 30 December 2025; Accepted 30 December 2025.

https://doi.org/10.53063/synsint.2025.54314

lead to excessive grain growth during sintering [2, 28, 29]. Additionally, oxide layers covering the surface of TiB_2 can cause significant grain growth during high-temperature sintering, resulting in reduced fracture toughness [30–32].

To date, numerous additives have been explored to enhance the properties of SiC ceramics. However, the creation of SiC-TiB_2 composites presents a suitable solution, combining the advantageous properties of both materials while addressing their respective weaknesses. This ceramic matrix composite, characterized by advanced composition and durability, has been investigated by Bucevac and his colleagues and is recommended for use in mechanical systems under high load, high speed, and high temperature conditions [33]. The inclusion of TiB_2 particles, which have a higher thermal expansion coefficient compared to the SiC matrix, can improve the fracture toughness of the system. Specifically, the presence of these particles results in greater contraction of the second-phase particles during cooling from the manufacturing temperature, compared to the SiC matrix. This discrepancy creates compressive residual stress around the particles, which reduces the tensile stress at the crack tip, ultimately leading to enhanced strength, thermal shock resistance, and fracture toughness [34–36]. Another significant benefit of incorporating TiB_2 particles in SiC matrices is the improvement of sintering capability, achieved by removing the oxide impurity during the sintering process [37].

In recent years, the properties of SiC-TiB_2 composites made using pressureless sintering, plasma spark sintering, and hot-pressing methods have been investigated [38–39]. But the need for high temperatures and modification of properties has not disappeared. In this regard, reinforced particles are used to improve properties. When examining methods for modifying the properties of ceramic composites or using reinforcing materials, one can divide them into two categories: single component and multi-component additives. Including reinforcing materials such as carbides, nitrides, and oxides [37]. The influence of carbon family members, such as graphite, graphene, graphene oxide, carbon fibers, and carbon nanotubes, on the mechanical properties of SiC and TiB_2 composites has been extensively studied. The promising results of these studies have been comprehensively discussed in the literature [38–41].

Chen et al. [42] investigated the effect of graphene nanoplatelets (GNPs) on dense SiC ceramics. The samples were fabricated using a liquid phase hot pressing (HP) process. The effect of GNPs content in the range of 0–3 wt% on the phase composition, microstructural evolution, and mechanical and thermal properties of SiC ceramics was analyzed in detail. With the increase of GNPs content from 0 to 3 wt%, the density and hardness of SiC/GNPs composites decreased uniformly, while the flexural strength, fracture toughness, and thermal conductivity increased initially and then decreased. The decrease in density and hardness is due to the low density and low hardness of GNPs themselves. The sample containing 1 wt% GNP has the highest relative density of 99.5% and a hardness of 26.3 GPa. The main strengthening and toughness mechanisms include fine-grain strengthening, dislocation strengthening, crack bridging, crack deflection, and crack termination. Razmjoo et al. [43] investigated the effect of graphene content on the mechanical properties of β-SiC in the presence of SiC nanoparticles, and sintering of composites at 2200 °C was investigated by pressureless sintering. Based on the results, the highest relative density of 99.04%, Young's modulus of 537.76 GPa, and fracture toughness of 5.73 $MPa.m^{1/2}$ were obtained in the sample containing 5 wt% nano-β-SiC and 1 wt% graphene. Also, the highest hardness was 29.97 GPa in the sample containing 5 wt% nano-β-SiC with 1 wt% additive. One of the mechanisms for improving the fracture toughness of α-SiC ceramics is the formation of cracks/bridging. Also, the difference in thermal expansion of the α-SiC mass and the reinforcements, which leads to the creation of material stresses between the matrix and reinforcement grains, results in improved mechanical properties (such as strength and fracture toughness).

Kovalčíková and colleagues [3] have investigated silicon carbide/graphene platelet (SiC/GPLs) composites with different weight percentages of GPLs fillers using hot pressing (HP) technology at 2100 °C. The effect of GPLs addition on fracture toughness and its mechanisms has been investigated. The highest fracture toughness was obtained in the sample containing 1 wt% GPLs with a fracture toughness of 4.4 $MPa.m^{1/2}$, a relative density of 99.7%, and a hardness of 20.98 GPa. The main sources of fracture were strength-reducing defects, pores at low platelet content, and the combination of pores and GPLs or clusters of GPLs particles in systems with higher platelet content. The fracture toughness increased due to activated hardening mechanisms, mainly in the form of crack bridging and crack branching, while crack deflection was limited.

Research shows [27] that using the plasma spark sintering method and reinforcing graphene nanosheets, the fracture toughness of a silicon carbide matrix composite is improved by 40% in a sample containing 2% by weight of graphene nanosheets.

Studies have shown that as a source of carbon, graphene provides the driving force for diffusional mass transport during sintering by reducing the ratio of grain boundary energy to surface energy [44–46]. Another role of graphene as a carbon source is that it reacts with the SiO_2 layer on the surface of SiC powder to form secondary SiC [46]:

$$SiO_2 + 3C \rightarrow SiC + 2CO(g) \quad (1)$$

Chen et al. [42] used carbon as a sintering additive to enhance the density of SiC and improve its purity. In their study, various carbon sources (graphitic carbon microsphere, carbon black, and flake graphite) were combined with B_4C through spark plasma sintering (SPS) at temperatures ranging from 1800 °C to 1900 °C. Their results showed that the SiC specimens prepared with graphitic carbon microspheres had a smaller crystallite size than those prepared with other types of carbon and exhibited high relative density, hardness, fracture toughness, and remarkable oxidation resistance. This was attributed to the lower oxygen content, better dispersion, and higher chemical reactivity of graphitic carbon spheres. In general, the use of carbon sources with high reactivity and good dispersion is an effective method in preparing SiC ceramics.

The discovery of graphene quantum dots in 2008 by Ponomarenko et al. [47] opened a new window in the world of materials. Graphene quantum dots, as a new member of the carbon family, are chemically and physically different from other carbon materials. Emerging materials graphene quantum dots, as the newest member of the large carbon family with dimensions smaller than 100 nm [48], have a high potential to participate in reactions and, by increasing reactivity, are effective in curing kinetics, sintering ability, and improving mechanical properties such as density and toughness. It is predicted that graphene quantum dot nanoparticles (GQDs) can act as very effective barriers to crack propagation (crack bridging and crack deflection) due to their very small size and high surface-to-volume ratio. This can lead to improved fracture toughness.

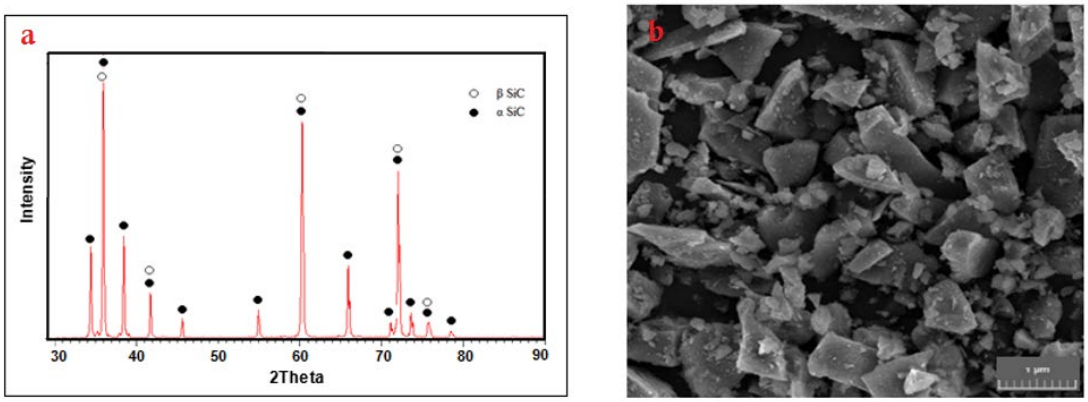

Fig. 1. a) XRD pattern of SiC and b) FESEM image of the morphology of the α-SiC powder.

In the author's previous research [49], the amount of graphene quantum dots below 1 wt% was investigated. According to the obtained results, 0.6 wt% GQD provided the optimal results. Therefore, in this study, the authors investigated the sintering behavior and the effect of different temperatures (2000, 2050, 2100, 2150, 2200 °C) on the microstructure, density, hardness, fracture toughness, etc. of pressure-sintered SiC-5TiB_2-0.6GQD composites. To further investigate the sintering process and analyze the results, the stability of the phases and possible reactions were evaluated thermodynamically.

2. Experimental procedure

2.1. Materials and methods

The required raw materials for this research include the α-silicon carbide (99%, China), titanium diboride (Chengdu Rong Feng, China), and graphene quantum dot powders. α-SiC has an average particle size of 0.8 µm For a better performance, 5% β-SiC was added to the raw material batch, as noticed in the X-ray patterns (Fig. 1).

XRD results of the grey-colored titanium diboride with an average particle size less than 8 µm is shown in Fig. 2. The applied graphene quantum dot was synthesized by a carbonization method, previously reported by Wu et al. [22] from L-glutamic acid (Merck, Germany), particles size of GQD is below 10 nm, and the HRTEM results are shown in Fig. 3.

Fig. 3 illustrates the particle size distribution, which confirms the uniform distribution of the graphene quantum dot particles and their spherical morphology. The particle distribution is also nearly uniform in terms of dimensions, and a detailed examination of the particle-size distribution curve reveals that the highest frequency of particle sizes occurs in the 3–6 nm range.

This research aims to investigate the effect of sintering temperature on the properties and the microstructure of SiC-5TiB_2-0.6GQD nanocomposite, obtained by the pressureless sintering method. Therefore, after scaling the powders, the milling process was conducted in a Teflon cup with zirconia balls and a ball-to-powder ratio of 10:1 at a rate of 200 rpm for 2 h. Then, the mixture was placed in an oven at 100 °C to remove the ethanol. Then, it was screened through a mesh of 500. The obtained powders were pressed under a uniaxial pressure of 80 MPa. The samples were sintered at 2000, 2050, 2100, 2150, and 2200 °C under an argon atmosphere for 2 h. The samples were subjected to various tests to investigate their mechanical and

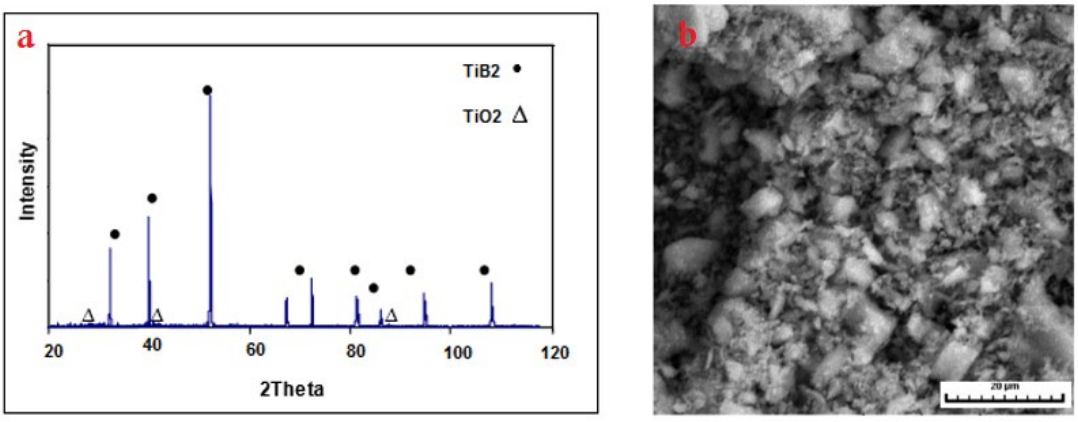

Fig. 2. a) XRD pattern of TiB_2 and b) FESEM image of the morphology of the TiB_2 powder.

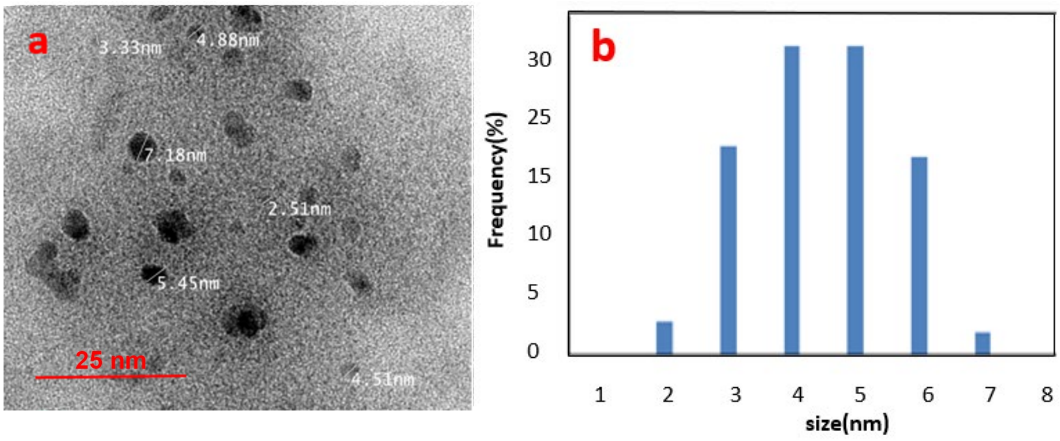

Fig. 3. a) HRTEM and b) particle size of GQD.

microstructural properties. We will examine each one below. The density of the samples was checked by the Archimedes method and based on the ASTM B311 standard. Microhardness was also calculated based on the ASTM 1327 standard. Also, to check the microstructure of the samples, they are polished and then etched with Murakami solution, and then imaging is done using the FESEM MIRA3 TESCAN-XMU model. The image was analyzed using the Material plus ver 4.1 software. It was also used for phase analysis of raw and sintered materials, an X-ray diffraction machine made in Italy with the 2000APD-GNR model. The X-ray diffraction pattern of the samples was obtained with a Cu-Kα beam, nickel filter, and a 40 kV accelerating voltage. To investigate the morphology of the surface of graphene quantum dots, high-resolution transmission electron microscopy was employed to examine the lattice structure and the lattice parameter. The measurements were conducted using an HRTEM with a 200 kV Schottky field-emission gun. Raman spectroscopy was performed to probe graphene quantum dots in the samples using an Ocean Optics system, with a laser wavelength of 532 nm.

3. Results and discussion

3.1. Phase analysis

Fig. 4 shows the XRD patterns of the SiC-5TiB_2-0.6GQD sample, sintered at 2100 and 2200 °C. As seen, SiC exists in the form of two allotropes, 6H and 4H, in the structure. The allotropes of 6H and 4H have also been reported in the article on the properties of SiC composites by Razmjoo [27]. From a comparison of graphs a and b, it can be seen that the peaks in graph b have shifted to the left compared to graph a, which is due to the higher sintering temperature and the resulting stresses. The thermodynamic results indicate some TiB_2, TiC, and B_4C in the final product, but not detected by the XRD due to the low amounts. Increasing the temperature enhanced the peak intensity, showing the complement of the sintering reaction.

The presence of graphene quantum dots in the composite sample sintered at 2000 °C was examined by Raman analysis (Fig. 5). Two characteristic peaks of SiC about 785 and 965 cm^{-1} were detected

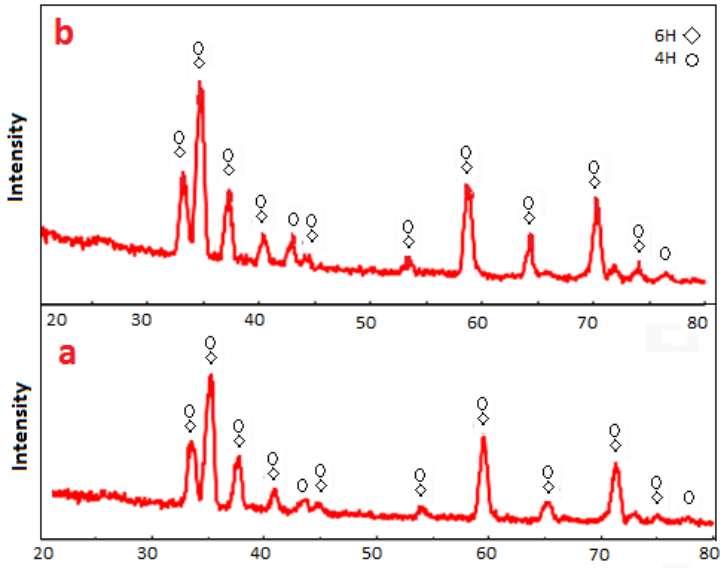

Fig. 4. XRD analysis of the samples sintered at a) 2100 and b) 2200 °C.

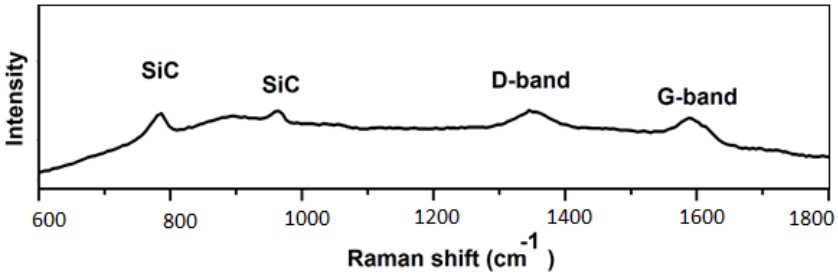

Fig. 5. Raman spectroscopies of the sample sintered at 2000 °C.

and the Raman peaks of GQD were also detected, the characteristic peaks of GQD about 1355 and 1580 cm^{-1} were directly detected. The specifications of the couriers have already been reported by some researchers [22, 38]. In this way, the presence of graphene quantum dot nanoparticles in the final structure of the sample was confirmed.

3.2. Microstructure studies

In the following, the microstructure of the sintered sample at 2000 °C and the effect of sintering temperature on grain size are investigated. As can be seen in the image of Fig. 6, the SiC background (dark gray), along with the distribution of TiB_2 particles (light gray) areas in the field, as well as the porosity of the black areas in the microstructure, can be seen with EDS analysis, and GQD particles smaller than 10 nm are also not visible in the structure.

In Fig. 7, the linear analysis of the sample sintered at 2050 °C is shown. As can be seen in the figure, carbon and silicon elements are observed in almost all points, which indicates the SiC field. The presence of TiB_2 enhancer is also confirmed by the presence of Ti and B elements in the analysis chart, and the presence of carbon element in amounts of more than 35 wt% in the beginning and end points, and its lack of significant reduction in the field confirms the homogeneous distribution of GQD and carbon in the field SiC composition.

The effect of different sintering temperatures on the microstructure of the samples is shown in Fig. 8. Almost all grains are elongated with increasing the amount of temperatures from 2000 to 2150 °C, the average length grain size of SiC increased from 6.81 to 8.42 µm and then decrease at 2200 °C to 7.67 µm. Elongated grains are mainly created by 6H–4H transformations. Changes in the grain morphology are factors that have grate influence on the mechanical properties [50]. Elongated of grains can trigger mechanisms such as deflection and bridging of cracks and fracture toughness is improved. Increasing the sinter temperature usually leads to increased thermal energy and atomic motion, which in turn leads to an increase in the grain growth rate. This phenomenon can be explained by the role of temperature is very effective in homogenization and dissolution processes. As the temperature is further increased and approaches 2200 °C, the grain size decreases. This phenomenon can be attributed to Zener pinning: the presence of graphene quantum dot reinforcing particles and their uniform distribution in the matrix hinder grain-boundary movement and can further limit or halt grain growth. The pinning force exerted by the secondary-phase particles counteracts surface and boundary diffusion, effectively suppressing abnormal grain growth at high temperatures [27]. Table 1 shows the results of investigating the effect of sintering temperature on SiC grains size. As the results of Table 1 show, increasing the sintering temperature increases atomic diffusion and causes grain growth by moving the grain boundaries. As a result, the average length and thickness of the grains increase. The growth in grain thickness is faster and as a result, the average aspect ratio decreases.

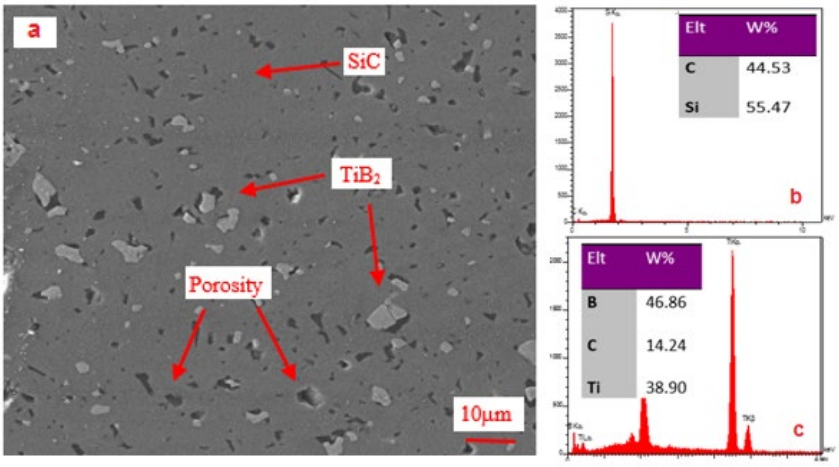

Fig. 6. a) FESEM micrograph of specimen sintered at 2050 °C, with b & c) the EDS analysis.

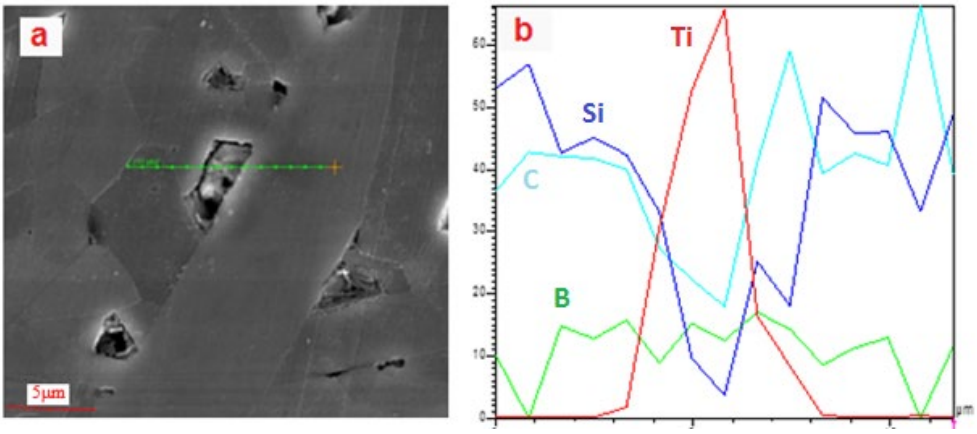

Fig. 7. Line scan analysis of the sample sintered at 2050 °C.

3.3. Relative density

Fig. 9 shows the density variations of the SiC-5TiB_2-0.6GQD composite according to the sintering temperature. As seen, the density variations are ascending with an increase in temperature, and the maximum relative density of 96.26% is obtained by reaching the temperature of 2150 °C.

Based on the diagram, we can conclude that the sintering process is

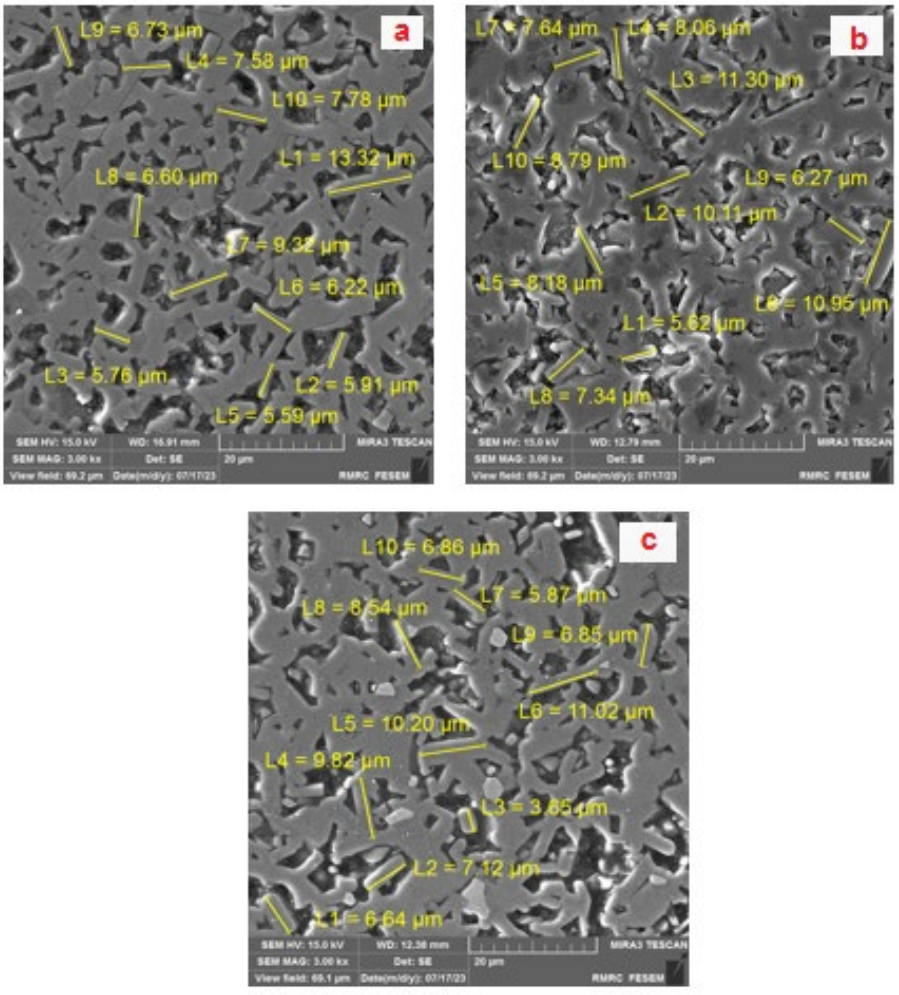

Fig. 8. FESEM images of samples sintered at a) 2050, b) 2150, and c) 2200 °C.

Table 1. Effect of temperature on morphology of elongated SiC grains in SiC-5TiB_2-0.6GQD composite.

Temperature (°C)	Average length (μm)	Average thickness (μm)	Average aspect ratio
2000	6.81±1.2	1.70±0.5	4.00
2050	7.48±3.1	1.83±0.4	4.15
2100	7.63±2.6	2.45±0.3	3.17
2150	8.42±2.1	2.81±0.5	3.00
2200	7.67±3.3	2.64±0.7	2.95

completed at 2150 °C and the maximum density is obtained at this temperature. On the other hand, the presence of a SiO_2 layer on the surface of silicon carbide particles is inevitable. This oxide layer can participate in the formation of the liquid phase. According to the research [44], if the amount of SiO_2 on the surface of SiC particles is optimized, the liquid phase is distributed more homogeneously between the SiC grains, which results in improved densification of samples. The decrease of pore size and their volume fraction are affective to the density level. The increase in temperature and the SiO_2 layer removal from the surface of the particles enhanced the surface energy of the powder, facilitating the mass transfer. An excessive increase in temperature up to 2200 °C would result in uncontrolled grain growth, a decreased density, the appearance of porosity, and the agglomeration of graphene quantum dot particles, and finally, the amount of density decreases.

3.4. Weight loss

Fig. 10 indicates the mass loss plot of the SiC-5TiB_2-0.6GQD composite versus the variations of sintering temperature. The plot follows a uniform slope with the increase in temperature. Increasing the temperature to values greater than 2150 °C shows a negative slope in the graph.

In Fig. 11a, composition changes based on sinter temperature are shown. In the diagram, it can be seen that the raw materials for making the final composite with the combination of SiC-5TiB_2-0.6GQD, which

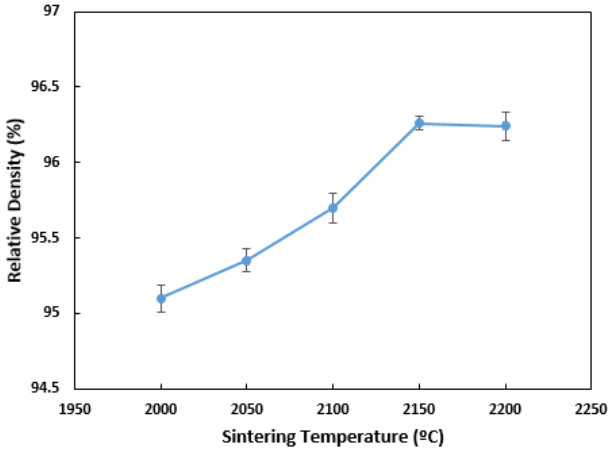

Fig. 9. Effect of temperature on the density of SiC-5TiB_2-0.6GQD composite.

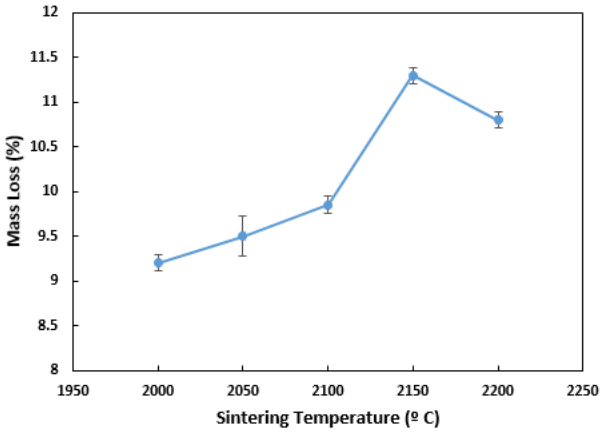

Fig. 10. Effect of temperature on the mass loss of SiC-5TiB_2-0.6GQD composite.

are used in construction in the form of phases SiC, TiB_2, and C, exist at zero-degree temperature. At the end of the sintering process, there are phases TiC, TiB_2, B, B_4C, C, and CO in the system, which do not appear in the XRD results due to their small amount. Due to the low amounts of Co and TiC present in the final product, it is not visible in the XRD analysis results. It also seems that the presence of CO in gaseous form in the microstructure is observed as porosity in the samples.

A noteworthy point is that the results of theoretical calculations will significantly enhance the understanding of the system's behavior at high temperatures. However, it is essential to keep in mind that these calculations are based on the thermodynamic behavior of materials, and other processes may occur in reality. Because in the calculations the system is considered closed, but in practice the furnace is under an argon atmosphere, and there is a possibility of any change in the test conditions.

The thermodynamic behavior of the two reactions in Table 2 predicts for the system. Based on the information from the Gibbs free energy diagram, it can be concluded that reaction 1 is dominant in the system in the temperature range of 2000 to 2100 °C, and CO gas is the only output of this system. However, with further increase in temperature and approaching 2200 °C, reaction 2 becomes dominant in the system, and based on that, in addition to CO gas, SiO is also formed and removed from the system. As a result, the system experiences a higher mass loss percentage.

Table 2. Comparison of the Gibbs energy values at different temperatures in SiC-5TiB_2-0.6GQD composite.

Temperature (°C)	ΔG (kJ)	Reactions
2000	-154.2	$SiO_2 + 3C = SiC + 2CO(g)$
2500	-310	
2000	-78.27	$SiC + 2SiO_2 = 3SiO(g) + CO(g)$
2500	-391.7	

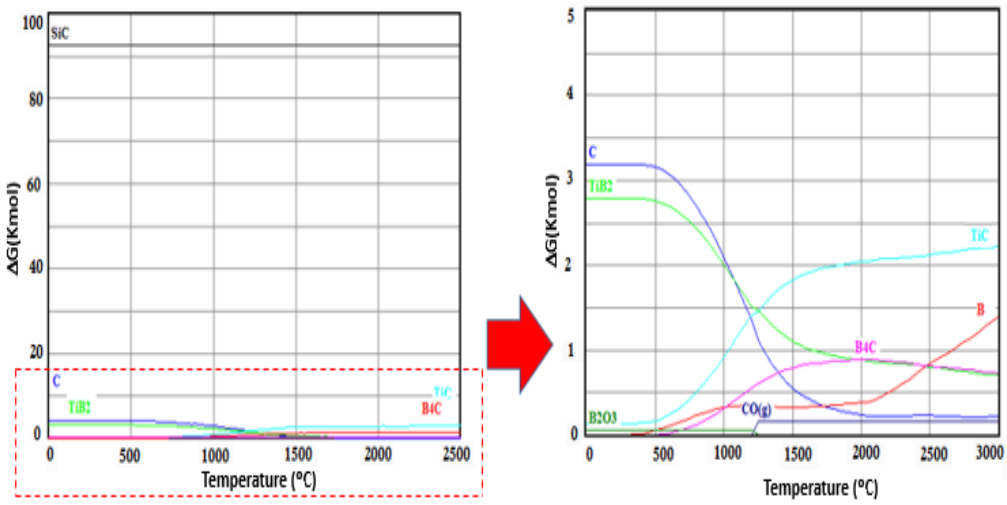

Fig. 11. Gibbs free energy changes of reactions in the SiC-TiB_2-GQD system in according to the temperature at 0.001 MPa pressure.

3.5. Hardness

In Fig. 12, the effect of different sintering temperatures on the hardness of samples is presented. As seen, hardness increases with increasing sintering temperature. The temperature is continuously enhanced up to 2150 °C, reaching a maximum point. The hardness is 28.65 GPa at this temperature. After that, the hardness plot experiences a descending trend with the increase in temperature and reaches 27.85 GPa. The highest hardness is related to the sample having the highest relative density.

The high surface-to-volume ratio of graphene quantum dots particles increases the contact between particles and accelerates the mass transfer and sintering process in the sample, reducing the porosity. Therefore, reducing the volume fraction of porosity in the sample leads to increased densification and, consequently, higher hardness. At values greater than 2150 °C, the increase in temperature acts as a driving force to remove oxide particles from the system, which is accompanied by the release of CO and SiO gas phases, leading to increased porosity, reduced density, and ultimately reduced hardness of the sample.

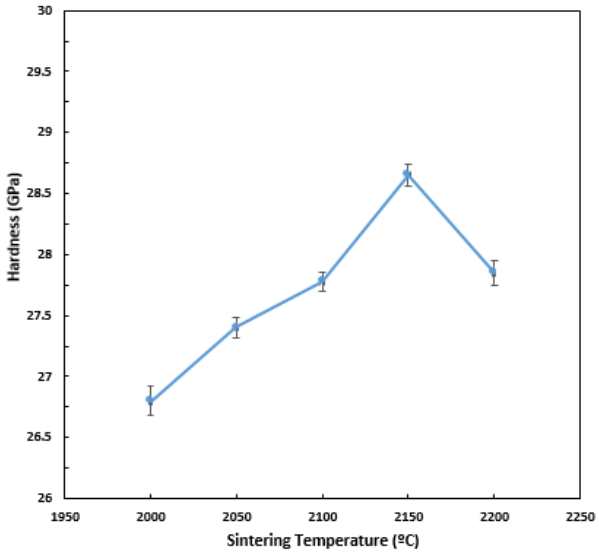

Fig. 12. Effect of temperature on hardness of SiC-5TiB_2-0.6GQD composite.

3.6. Elastic modulus

In Elastic modulus investigations, some parameters such as the type of material, the constituent phases, density, and porosity are important. Eq. 2 shows the relationship between porosity (P) and sound velocity (E).

$$E = 460\times(1–P)/(1+2.999P) \quad (2)$$

A review of the data recorded in Table 3 shows that due to the high porosity in the 2000 °C sample, it was not possible to measure the modulus and speed of sound in this sample. As the firing temperature increases further due to grain growth, porosity and defects in the system decrease (Fig. 13 also shows this), the sample becomes denser, resulting in a higher modulus. As the temperature increases further and reach 2200 °C, the elastic modulus decreases due to the appearance of more porosities and a decrease in density. With further increase in temperature and reaching 2200 °C, the elastic modulus decreases due to the appearance of more porosities and a decrease in density.

Table 3. Comparison of porosity, speed of sound, and elastic modulus at different temperatures.

Temperature (°C)	Elastic modulus (GPa)	Speed sound (m/s)	Porosity (%)
2000	-	-	17.1
2050	200.43	8357	10.6
2100	486.31	12586	7.96
2150	513.30	12398	2.37
2200	483.20	12156	2.70

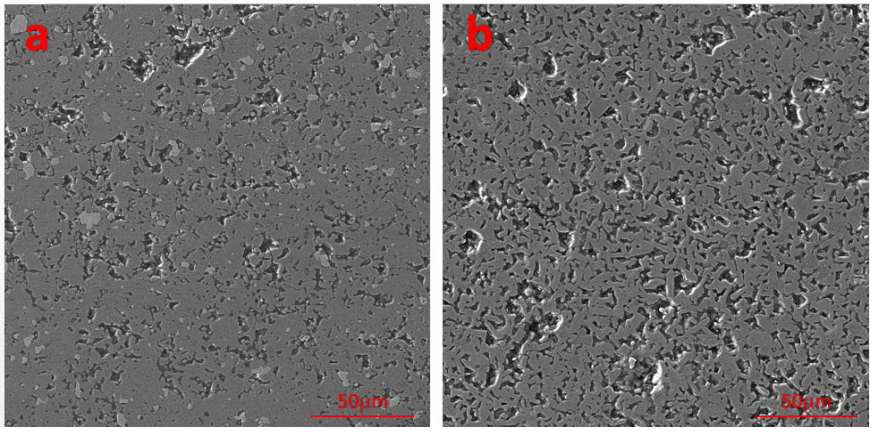

Fig. 13. FESEM images of the distribution of porosity in the matrix of samples sintered at a) 2050 and b) 2150 °C.

3.7. Fracture toughness

Fig. 14 shows the variations of fracture toughness as a function of the sintering temperature. As can be seen, increasing the sintering temperature resulted in the maximum fracture toughness, the maximum data being 4.1 MPa.m$^{1/2}$ (at 2150 °C) with a relative improvement of 29%, compared to the initial temperature (2000 °C) 3.18 MPa.m$^{1/2}$. Further increase in sintering temperature to 2200 °C resulted in a fracture toughness of 3.82 MPa.m$^{1/2}$ with a decrease of 7%. Strength, grain size, porosity, and microstructure affect fracture toughness. The improvement in fracture toughness is also consistent with the results of density measurements. When the sintering temperature increases, the sintering process is complete, so that at 2150 °C, the sintering process is complete, and the pore volume in the system reaches its minimum value. Therefore, considering the coincidence of grain growth with increasing temperature and improving microstructure, fracture toughness is expected to have a maximum value at 2150 °C. Further increase in temperature with increasing porosity increases potential sites for crack formation. Therefore, the reason for the lower resistance to indentation fracture of the sample sintered at 2200 °C compared to 2150 °C is the higher porosity. It is also possible that their size reaches the critical size required for fracture initiation. Of course, researchers report grain size and elongation as other parameters affecting fracture toughness. Due to the weak bonding between SiC grains and the boundary phase, the crack propagation path is mainly along grain boundaries. When the crack tip reaches a grain during crack propagation and growth, the grain acts as an elastic bridge and breaks during crack propagation, leading to intergranular fracture [27].

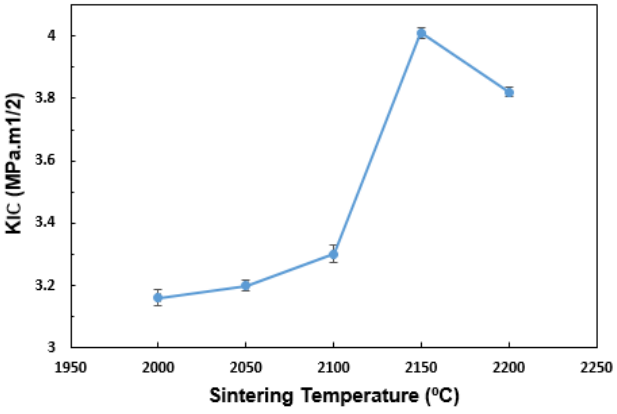

Fig. 14. Effect of temperature sintering on fracture toughness of SiC-5TiB_2-0.6GQD composite.

3.8. Toughening mechanisms

The mechanisms of increasing toughness mainly include crack deflection, crack bridging, and crack branching [27]. Fig. 15 shows the FESEM images of the crack growth mechanism in sintered samples that were sintered at 2150 °C.

The gaseous products of the reactions occurring in the system cause the formation of porosity in the composite structure. As can be seen in the images (Fig. 15a), crack nucleation in the leads to intergranular fracture and provides suitable conditions for longer paths by forming open and torn areas. This reduces the fracture energy and relatively increases the fracture toughness.

The presence of TiB_2 and graphene quantum dots particles in the field of SiC causes the crack to deviate from these particles, and the toughness improves with the energy consumption of the crack (Fig. 15b).

The images of the fracture surfaces of the samples sintered at 2000 °C and 2150 °C are shown in Fig. 16.

As seen, increasing the temperature has resulted in grain growth, a porosity reduction, and improved fracture toughness through an accomplished sintering process. When the strength of the grain boundary increases, an intergranular fracture occurs by eliminating a portion of the grains, sliding, and layering, called the cleavage steps. The Cleavage stepping improves the fracture toughness of the composite by prolonging the propagation path of the cracks and consuming more energy for the fracture [51]. An example of this mechanism is shown in Fig. 16.

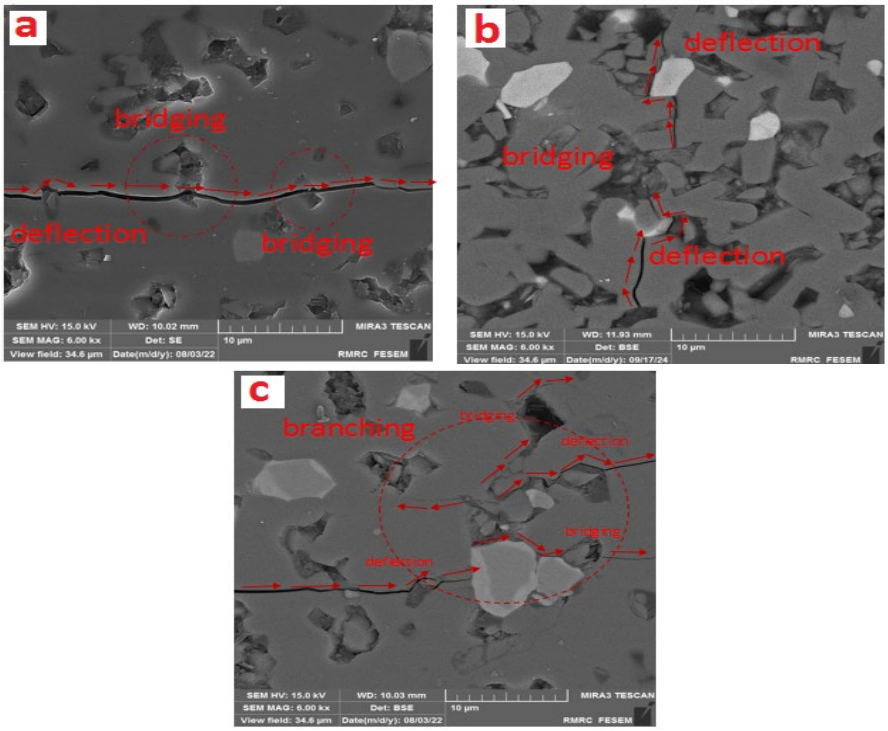

Fig. 15. FESEM images of crack propagation path and the relevant toughening mechanisms of sample sintered at 2150 °C.

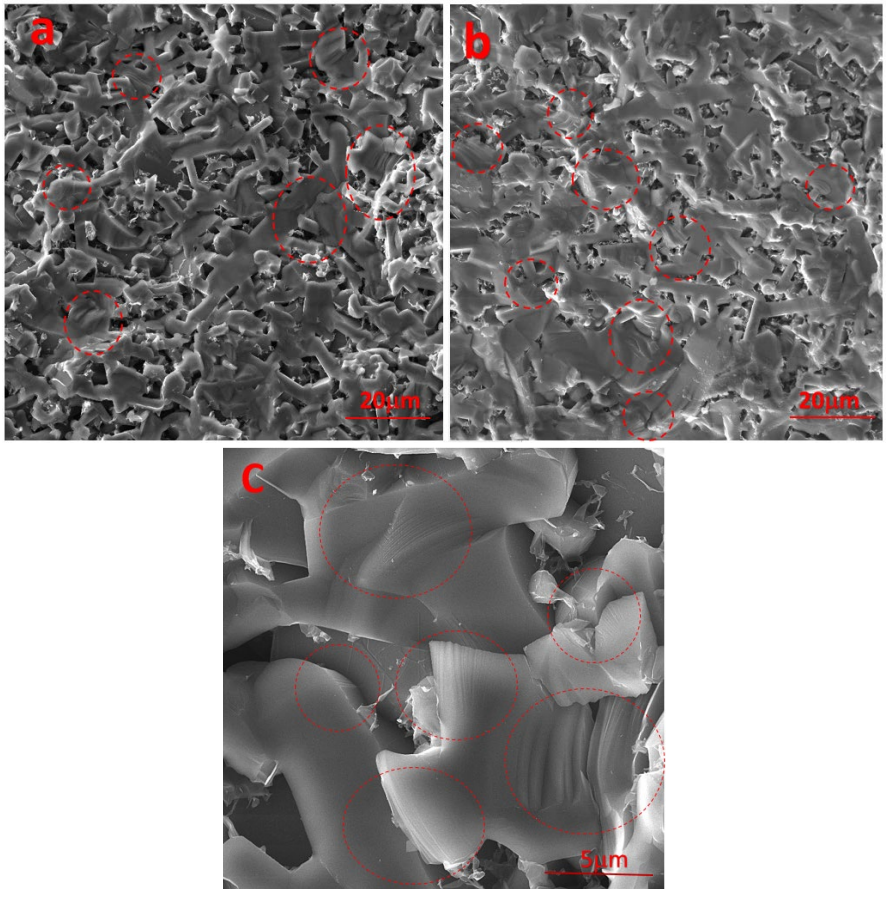

Fig. 16. FESEM images of the fracture surface of samples sintered at a) 2000, b & c) 2150 °C.

4. Conclusions

- The investigation of phase analysis using X-rays shows that with increasing temperature, the allotropy of α-SiC changes from 6H to 4H allotropy and the structure is subjected to lattice strain.
- The study of thermodynamic reactions shows that the presence of SiO and CO gas phases is the cause of porosity formation in the microstructure.
- The appearance of D and G bands in Raman analysis confirms the presence of graphene quantum dot particles in the structure.
- The results showed that the sample sintered at 2150 °C has the highest relative density, elastic modulus, hardness, and fracture toughness of 96.26%, 513.3 GPa, 28.65 GPa, and 4.1 MPa.$m^{1/2}$, respectively.

CRediT authorship contribution statement

Maryam Nazari: Conceptualization, Investigation, Software.
Hamid Reza Baharvandi: Writing – review & editing, Supervision, Methodology, Validation, Writing- original draft.
Nasser Ehsani: Data curation, Methodology, Software, Validation.

Data availability

The data underlying this article will be shared on reasonable request to the corresponding author.

Declaration of competing interest

The authors declare that they have no known competing financial interests or personal relationships that could have appeared to influence the work reported in this paper.

Funding and acknowledgment

This research did not receive any specific grant from funding agencies in the public, commercial, or not-for-profit sectors.

References

[1] H.K. Pant, D. Debnath, S. Chakraborty, M.F. Wani, P.K. Das, Mechanical and tribological properties of spark plasma sintered SiC–TiB2 and SiC–TiB2–TaC composites: effects of sintering temperatures (2000° C and 2100° C), J. Tribol. 140 (2018) 011608. https://doi.org/10.1115/1.4037068.

[2] I. Akin, O. Kaya, Microstructures and properties of silicon carbide- and graphene nanoplatelet-reinforced titanium diboride composites, J. Alloys Compd. 729 (2017) 949–959. https://doi.org/10.1016/j.jallcom.2017.09.244.

[3] A. Kovalčíková, P. Tatarko, R. Sedlak, D. Medve, Z. Chlup, et al., Mechanical and tribological properties of TiB2-SiC and TiB2-SiC-GNPs ceramic composites, J. Europ. Ceram. Soc. 40 (2020) 4860–4871. https://doi.org/:10.4149/km-2019-6-435.

[4] H.M. Kim, Y.W. Kim, Low temperature pressureless sintering of silicon carbide ceramics with alumina–yttria–magnesia-calcia, J. Ceram. Soc. Jpn. 127 (2019) 207–214. https://doi.org/10.2109/jcersj2.19024.

[5] E. Ciudad, O. Borrero-López, F. Rodríguez-Rojas, A.L. Ortiz, F. Guiberteau, Effect of intergranular phase chemistry on the sliding-wear resistance of pressure less liquid-phase-sintered α- SiC, J. Europ. Ceram. Soc. 32 (2012) 511–516. https://doi.org/10.1016/j.jeurceramsoc.2011.09.011.

[6] A. Jung-Hye Eom, A. Young-Wood Kim, S. In-Hyuck, Effects of the initial α-SiC content on the microstructure, mechanical properties, and permeability of macro porous silicon carbide ceramics, J. Europ. Ceram. Soc. 32 (2012) 1283–1290. https://doi.org/10.1016/j.jeurceramsoc.2011.11.040.

[7] J. Yu, G. Zhao, C. Zhang, L. Chen, Dynamic evolution of grain structure and micro-texture along a welding path of aluminum alloy profiles extruded by porthole dies, J. Mater. Sci. Eng: A. 682 (2017) 679–690. https://doi.org/10.1016/j.msea.2016.11.089.

[8] S. Zhu, M. Mizuno, Y. Kagawa, Y. Mutoh, Monotonic tension, fatigue and creep behavior of SiC-fiber-reinforced SiC-matrix composites: a review, J. Compos. Sci. Technol. 59 (1999) 833–851. https://doi.org/10.1016/S0266-3538(99)00014-7.

[9] S. Somiya, Y. Inomata, Silicon Carbide Ceramics: Gas phase reactions, fibers and whisker, joining, Springer Dordrecht. (1991).

[10] H. Liang, X. Yao, Z. Huang, Y. Zeng, B. Su, The relationship between microstructure and flexural strength of pressureless liquid phase sintered SiC ceramics oxidized at elevated temperatures, Ceram. Int. 42 (2016) 13256–13261. https://doi.org/10.1016/j.ceramint.2016.05.125.

[11] R. Sedlák, A. KovalĽíková, V. Girman, E. Múdra, P. Rutkowski, et al., Fracture characteristics of SiC/graphene platelet composites, J. Europ. Ceram. Soc. 37 (2017) 4307–4314. https://doi.org/10.1016/j.jeurceramsoc.2017.04.067.

[12] D. Bucevac, B. Matovic, S. Boskovic, S. Zec, V. Krstic, Pressureless sintering of internally synthesized SiC-TiB2 composites with improved fracture strength, J. Alloys Compd. 509 (2011) 990–996. https://doi.org/10.1016/J.JALLCOM.2010.09.152.

[13] S. Li, X. Luo, C. Wei, P. Gao, P. Wang, L. Zhou, Enhanced strength and toughness of silicon carbide ceramics by graphene platelet-derived laminated reinforcement, J. Alloys Compd. 834 (2020) 155252. https://doi.org/10.1016/j.jallcom.2020.155252.

[14] K. Suzuki, M. Sasaki, Effects of sintering atmosphere on grain morphology of liquid-phase-sintered SiC with Al2O3 additions, J. Europ. Ceram. Soc. 25 (2005) 1611–1618. https://doi.org/10.1016/j.jeurceramsoc.2004.06.007.

[15] Y. Zhu, H. Cheng, Y. Wang, R. An, Effects of carbon and silicon on microstructure and mechanical properties of pressureless sintered B4C/TiB2 composites, J. Alloys Compd. 772 (2019) 537–545. https://doi.org/10.1016/j.jallcom.2018.09.129.

[16] S. Dong, Y. Katoh, A. Kohyama, Preparation of SiC/SiC composites by hot pressing, using Tyranno-SA fiber as reinforcement, J. Am. Ceram. Soc. 86 (2003) 26–32. https://doi.org/10.1111/j.1151-2916.2003.tb03272.x.

[17] R. Ruh, A. Zangvil, Composition and Properties of Hot-Pressed SiC-AIN Solid Solutions, J. Am. Ceram. Soc. 65 (1982) 260–265. https://doi.org/10.1590/S0366-69132000000100002.

[18] P. Sahani, S.K. Karak, B. Mishra, D. Chakravarty, D. Chaira, Effect of Al addition on SiC–B4C cermet prepared by pressureless sintering and spark plasma sintering methods, Int. J. Refract. Met. Hard Mater. 57 (2016) 31–41. https://doi.org/10.1016/j.ijrmhm.2016.02.005.

[19] H. Ghezelbash, A. Zeinali, N. Ehsani, H.R. Baharvandi, The effect of aluminum additive on pressureless sintering of SiC, J. Aust. Ceram. Soc. 55 (2019) 903–911. https://doi.org/:10.1007/s41779-019-00310-0.

[20] D. Bucevac,V. Krstic, Microstructure–mechanical properties relations in SiC–TiB2 composite, J. Mater. Chem. Phys. 133 (2012) 197–204. https://doi.org/10.1016/j.matchemphys.2012.01.007.

[21] S. Prochazka, Sintering of silicon carbide, Mass transport phenomena in ceramics, Springer, Boston, MA. (1975) 421–431. https://doi.org/10.1007/978-1-4684-3150-6_28.

[22] X. Wu, F. Tian, W. Wang, J. Chen, M. Wu, J.X. Zhao, Fabrication of highly fluorescent graphene quantum dots using L-glutamic acid for in vitro/in vivo imaging and sensing, J. Mater. Chem. C. 1 (2013) 4676–4684. https://doi.org/10.1039/C3TC30820K.

[23] A. Malinge, A. Coupé, L. Petitcorps, R. Pailler, Pressureless sintering of beta silicon carbide nanoparticles, J. Europ. Ceram. Soc. 32 (2012) 4393–400. https://doi.org/10.1016/j.jeurceramsoc.2012.06.008.
[24] D. Ahmoye, V.D. Krstic, Reaction sintering of SiC composites with in situ converted TiO2 to TiC, J. Mater. Sci. 50 (2015) 2806–2812. https://doi.org/10.1007/s10853-015-8838-y.
[25] M. Khodaei, The effect of TiO2 additive on sinterability and properties of SiC- Al2O3-Y2O3 composite system, Ceram. Int. 44 (2018) 16535–16542. http://dx.doi.org/10.1016/j.ceramint.2018.06.073.
[26] W. Zhi, X. Bing, Z.H. Wenya, S. Guodong, W. Zhanjun, Thermophysical properties of TiB2\SiC ceramics from 300 °C to 1700 °C, Int. J. Refract. Met. Hard Mater. 41 (2013) 609–613. http://dx.doi.org/10.1016/j.ijrmhm.2013.08.001.
[27] A. Razmjoo, H.R. Baharvandi, N. Ehsani, αSiC-βSiC-graphene composites, Sci. Rep. 13 (2023) 4306. https://doi.org/10.1038/s41598-023-31539-2.
[28] I. Akin, M. Hotta, F.C. Sahin, O. Yucel, G. Goller, T. Goto, Microstructure and densification of ZrB2–SiC composites prepared by spark plasma sintering, J. Europ. Ceram. Soc. 29 (2009) 2379–2385. https://doi.org/10.1016/j.jeurceramsoc.2009.01.011.
[29] Y. Zhu, D. Luo, Z. Li, Y. Wang, H. Cheng, et al., Effect of sintering temperature on the mechanical properties and microstructures of pressureless-sintered B4C/SiC ceramic composite with carbon additive, J. Alloys Compd. 820 (2020) 153153. https://doi.org/10.1016/j.jallcom.2019.153153.
[30] P. Miranzo, C. Ramírez, B. Román-Manso, L. Garzón, H.R. Gutiérrez, et al., In situ processing of electrically conducting graphene/SiC nanocomposites, J. Europ. Ceram. Soc. 33 (2013) 1665–1674. https://doi.org/10.1016/j.jeucreamsoc.2013.01.021.
[31] D. Bucevac, B. Matovic, B. Babic, V. Krstic, Effect of post-sintering heat treatment on mechanical properties and microstructure of SiC–TiB2 composites, J. Mater. Sci. Eng. A. 528 (2011) 2034–2041. https://doi.org/10.1016/j.msea.2010.11.022.
[32] M. Khodaei, O. Yaghobizadeh, H.R. Baharvandi, A.A. Shahraki, The effect of nano-TiO2 additions on the densification and mechanical properties of SiC-matrix composite, Ceram. Int. 46 (2020) 6477–6483. https://doi.org/10.1016/j.ceramint.2019.11.128.
[33] D. Bucevac, S. Boskovic, B. Matovic, V. Krstic, Toughening of SiC matrix with in-situ created TiB2 particles, Ceram. Int. 36 (2010) 2181–2188. https://doi.org/10.1016/j.ceramint.2010.06.001.
[34] S.N. Grigoriev, Y. Pristinskiy, T.N. Soe, A. Malakhinsky, M. Mosyanov, et al., Processing and Characterization of Spark Plasma Sintered SiC-TiB2-TiC Powders, Materials (Basel). 15 (2022) 1946. https://doi.org/10.3390/ma15051946.
[35] Y. Huang, D. Jiang, X. Zhang, Z. Liao, Z. Huang, Enhancing toughness and strength of SiC ceramics with reduced graphene oxide by HP sintering, J. Europ. Ceram. Soc. 38 (2018) 4329–4337. https://doi.org/10.1016/j.jeurceramsoc.2018.05.033.
[36] T. Tani, Processing, microstructure and properties of in-situ reinforced SiC matrix composites, Compos. A: Appl. Sci. Manuf. 30 (1999) 419–423. https://doi.org/10.1016/S1359-835X(98)00129-8.
[37] C. Blanc, F. Thevenot, D. Goeuriot, Microstructural and mechanical characterization of SiC-submicron TiB2 composites, J. Europ. Ceram. Soc. 19 (1999) 561–569. https://doi.org/10.1016/S0955-2219(98)00227-1.
[38] M. Khodaei, O. Yaghobizadeh, A.A. Shahraki, S. Esmaeeli, Investigation of the effect of Al2O3–Y2O3–CaO (AYC) additives on sinterability, microstructure and mechanical properties of SiC matrix composites: a review, J. Refract. Met. Hard Mater. 78 (2019) 9–26. https://doi.org/10.1016.jijr.mhm.2018.08.008.
[39] M. Belmonte, A. Nistal, P. Boutbien, B. Román-Manso, M.I. Osendi, P. Miranzo, Toughened and strengthened silicon carbide ceramics by adding graphene-based fillers, J. Scr. Mater. 113 (2016) 127–130. https://doi.org/10.1016/j.scriptamat.2015.10.023.
[40] S. Tang, J. Deng, S. Wang, W. Liu, Fabrication and characterization of an ultra-high-temperature carbon fiber-reinforced ZrB2–SiC matrix composite, J. Am. Ceram. Soc. 90 (2007) 3320–3322. https://doi.org/10.1111/j.1551-2916.2007.01876.x.
[41] K.F. Chan, M.H. Zaid, M.S. Mamat, S. Liza, M. Tanemura, Y. Yaakob, Recent developments in carbon nanotubes-reinforced ceramic matrix composites: A review on dispersion and densification techniques, Crystals. 11 (2021) 457. https://doi.org/10.3390/cryst11050457.
[42] C. Chen, X. Han, H. Shen, Y. Tan, H. Zhang, et al., Preferentially oriented SiC/graphene composites for enhanced mechanical and thermal properties, Ceram. Int. 46 (2020) 23173–23179. https://doi.org/10.1016/j.ceramint.2020.06.097.
[43] A. Razmjoo, H.R. Baharvandi, N. Ehsani, The effect of graphene addition on the properties of SiC ceramics—a review, J. Aust. Ceram. 58 (2022) 437–460. https://doi.org/10.1007/s41779-022-00701-w.
[44] S. Prochazka, R.M. Scanlan, Effect of boron and carbon on sintering of SiC, J. Am. Ceram. Soc. 58 (1975) 72. https://doi.org/10.1111/j.1151-2916.1975.tb18990.x.
[45] H. Yang, L. Zhang, X. Guo, X. Zhu, X. Fu, Pressureless sintering of silicon carbide ceramics containing zirconium diboride, Ceram. Int. 37 (2011) 2031–2035. https://doi.org/10.1016/j.ceramint.2011.01.048.
[46] G.H. Wroblewska, E. Nold, F. Thümmler, The role of boron and carbon additions on the microstructural development of pressureless sintered silicon carbide, Ceram. Int. 16 (1990) 201–209. https://doi.org/10.1016/j.ceramint.2024.01.045.
[47] L.A. Ponomarenko, F. Schedin, M.I. Katsnelson, R. Yang, E.W. Hill, et al., Chaotic dirac billiard in graphene quantum dots, Science. 320 (2008) 356–358. https://doi.org/10.1126/science.115466.
[48] P. Tian, L. Tang, K.S. Teng, S.P. Lau, Gaphene quantum dots from chemistry to applications, Mater. Today Chem. 10 (2018) 221–258. https://doi.org/10.1016/j.mtchem.2018.09.007.
[49] M. Nazari, H.R. Baharvandi, N. Ehsani, Investigating the Effect of Chemical Composition and Sintering Temperature on Mechanical Properties of SiC-5TiB2 Nano Composite Reinforced by Graphene Quantum dot using Taguchi Test Design Method, J. Adv. Mater. Eng. 2 (2023) 69–84. https://doi.org/10.47176/JAME.42.2.1034.
[50] M. Khodaei, O. Yaghobizadeh, H.R. Baharvandi, S. Esmaeeli, H. Javi, The effect of Cr2O3 additions on sinter ability and mechanical properties of liquid-phase sintered SiC ceramics, J. Alloys Compd. 829 (2020) 154501. https://doi.org/10.1016/j.jallcom.2020.154501.
[51] F. Ghafuri, M. Ahmadian, R. Emadi, M. Zakeri, Effect of SPS parameters on the densification and mechanical properties of TiB2-SiC composites, Ceram. Int. 45 (2019) 10550–10557. https://doi.org/10.1016/j.ceramint.2019.02.119.